Bio-Driven Cell Region Detection in Human Embryonic Stem Cell Assay

Benjamin X. Guan, Bir Bhanu, Prue Talbot, and Sabrina Lin

Abstract—This paper proposes a bio-driven algorithm that detects cell regions automatically in the human embryonic stem cell (hESC) images obtained using a phase contrast microscope. The algorithm uses both statistical intensity distributions of foreground/hESCs and background/substrate as well as cell property for cell region detection. The intensity distributions of foreground/hESCs and background/substrate are modeled as a mixture of two Gaussians. The cell property is translated into local spatial information. The algorithm is optimized by parameters of the modeled distributions and cell regions evolve with the local cell property. The paper validates the method with various videos acquired using different microscope objectives. In comparison with the state-of-the-art methods, the proposed method is able to detect the entire cell region instead of fragmented cell regions. It also yields high marks on measures such as Jacard similarity, Dice coefficient, sensitivity and specificity. Automated detection by the proposed method has the potential to enable fast quantifiable analysis of hESCs using large data sets which are needed to understand dynamic cell behaviors.

Index Terms—Automated detection, bioinformatics, bio-driven, human embryonic stem cell (hESC)

1 Introduction

Human embryonic stem cells (hESCs) are pluripotent cells derived from the inner cell mass of blastocysts, and in culture, they closely resemble epiblast cells of gastrulating embryos [1], [2]. Due to fact that hESCs have the ability to self renew indefinitely and to differentiate into all three germ layers (ectoderm, endoderm, and mesoderm), they are widely used in research designed to tap their potential for treating degenerative diseases. In addition, hESCs provide one of the best models currently available for assessing the toxicity of environmental chemicals on prenatal development [3], [4].

Application of video bioinformatics tools to hESC problems can greatly accelerate research in both regenerative and preventive medicine. As an example, a video analysis method for quantifying the rate of hESC colony growth was used to evaluate the toxicity of cigarette smoke from conventional and harm reduction cigarettes [5], [6]. The hESCs were imaged over time using a high content Nikon BioStation IM incubation unit equipped with a phase contrast microscope. Time-lapse videos were evaluated quantitatively for colony growth during treatment with cigarette smoke. Analysis showed that side-stream smoke from "harm reduction" brands of cigarettes was as harmful as or even more harmful than side-stream smoke from a conventional brand [5].

Cell region detection using the BioStation's cell analysis software is done either manually or in a semi-automatic manner [6]. The fastest rate at which BioStation IM can collect data is one frame per two seconds. In the current study, a new video bioinformatics tool is developed to further enhance the analysis of hESC video data. With this new tool, cell regions are detected using a bio-driven algorithm that uses a mixture of two Gaussians and exploits properties of hESCs. Once cell regions are detected, quantitative data can be utilized to determine the rate of hESC growth and numerous other parameters related to it such as its blebbing and attachment behavior. Therefore, high sensitivity and specificity on cell region detection are significant. Most importantly, the proposed method requires only 1.2 seconds of processing time per frame on a laptop with a Intel(R) Core 2 Duo CPU processor that runs at 2.53 GHz, it can perform cell analysis concurrently with the BioStation which is collecting live video data. The establishment of an automated and accurate cell detection tool is valuable and necessary for studying dynamic processes in hESCs.

- *B.X. Guan and B. Bhanu are with the Center for Research in Intelligent Systems and the Department of Electrical Engineering, University of California-Riverside, Riverside, CA 92521. E-mail: xguan001@ucr.edu, bhanu@cris.ucr.edu.*
- *P. Talbot and S. Lin are with the Stem Cell Center, University of California-Riverside, Riverside, CA 92521. E-mail: {talbot, sabrina.lin}@ucr.edu.*

Manuscript received 31 Aug. 2013; revised 10 Jan. 2014; accepted 31 Jan. 2014. Date of publication 18 Feb. 2014; date of current version 5 June 2014.
For information on obtaining reprints of this article, please send e-mail to: reprints@ieee.org, and reference the Digital Object Identifier below.
Digital Object Identifier no. 10.1109/TCBB.2014.2306836

2 Related Work and Contributions

K-means algorithm and mixture of Gaussians using an Expectation-Maximization (EM) algorithm are widely used techniques for image segmentation. K-means segmentation algorithm by Tatiraju and Mehta [7] considered each pixel intensity value as an individual observation. It partitions these observations into K clusters in which each observation belongs to the cluster with the nearest mean intensity value [8], [9]. However, the method does not consider the intensity distribution of its clusters. In contrast, the mixture of Gaussians segmentation method using the EM (MGEM) algorithm proposed by Farnoosh and Zarpak [10] depends heavily on intensity distribution models to group the image data. The MGEM method assumes the image's intensity distribution can be represented by multiple Gaussians [7], [11], [12]. However, it does not take into account the neighborhood information. As a result, segmented regions obtained by the above algorithms lack connectivity with the pixels within their neighborhoods. This lack of connectivity of a pixel with its neighborhood pixels is due to the following two characteristics of hESC images (see Fig. 1): i) an incomplete halo surrounds the cell body; ii) cell body intensity values are similar to the substrate intensity values [13].

State of the art CL-Quant software [14] for bioinformatic image analysis requires users to make a recipe for the experimental data and the recipe is created with the data itself. It is semi-automatic, and its performance is heavily depended on the recipe maker. Our proposed method is intended to solve the connectivity problems by using cell property as well as the cell and substrate intensity distributions. The cell property manifests itself in spatial information where cell regions have a high intensity variation. This variation in cell region is due to the organelles inside the cell. We evolve the cell regions based on spatial information until the optimal intensity distributions of background (substrate) and foreground (hESCs) regions are obtained. The optimization is done on the original image and the spatial evolution is based on the spatial characteristic. The proposed method is bio-driven, fast and automated.

3 Technical Approach

In this section, we first explain the optimization metric modeled as a mixture of two Gausians, and its convergence. We then elaborate on hESC property as spatial information. The handling of noise and over-segmentation are also discussed in this section. For the convenience of a reader, a summary of the symbols used in paper is provided in Table 1.

3.1 Optimization Metric

The hESCs were cultured *in vitro* using methods described in detail previously [15]. The hESCs are grown in culture dishes coated with a layer of substrate (Matrigel). The substrate becomes the background after the hESCs are placed on its surface. Therefore, we

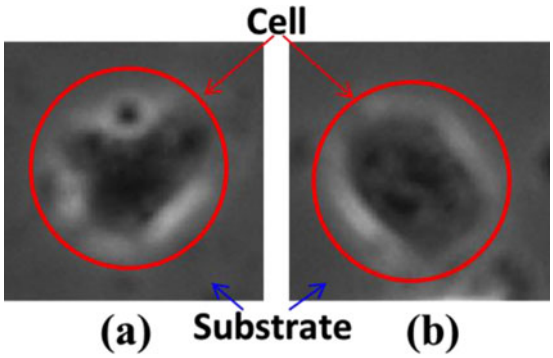

Fig. 1. (a)-(b). Cells with incomplete halo and similar substrate intensity values.

model a hESC image with two regions of interest: foreground and background. Fig. 2 shows that the intensity distributions of these regions are similar to a mixture of two Gaussians with different means and variances. Consequently, we model the intensity distribution of foreground (cell region with a mean μ_f and variance σ_f^2) and background (substrate region with a mean μ_b and variance σ_b^2) as the mixture of two Gaussians. Fig. 3 shows our model.

With this model, we then want to maximize the absolute difference of two mean-to-variance ratios (MVRs); the absolute difference of the foreground MVR and background MVR. The MVRs of the foreground and background data sets are calculated by the following equations [16]:

$$MVR_f = \frac{\mu_f}{\sigma_f^2}, \tag{1}$$

$$MVR_b = \frac{\mu_b}{\sigma_b^2}, \tag{2}$$

where MVR_f and MVR_b are the MVRs for the foreground and background data sets, respectively.

The optimization metric M is formulated as

$$M = \left|MVR_f - MVR_b\right|. \tag{3}$$

Substituting (1) and (2) into (3), we get the following:

$$M = \left|\frac{\mu_f}{\sigma_f^2} - \frac{\mu_b}{\sigma_b^2}\right|. \tag{4}$$

Equation (4) shows the metric that is used to determine how much the cell region data are different from the substrate region data. Since the algorithm is spatially evolving the foreground region from the initial high intensity variation region by a mean filter at each iteration, the foreground mean and variance are approaching to the background mean and variance. The limit of M is 0 as $\frac{\mu_f}{\sigma_f^2}$ approaches to $\frac{\mu_b}{\sigma_b^2}$. Therefore, our problem becomes finding M_{opt} which is the optimal value for metric M, and the corresponding equation is described below:

$$M_{opt} = \max_{\mu_f,\sigma_f^2,\mu_b,\sigma_b^2} M\left(\mu_f, \sigma_f^2, \mu_b, \sigma_b^2\right). \tag{5}$$

M_{opt} finds the parameters that maximize the difference between foreground and background data.

TABLE 1
Definition of the Symbols Used in This Paper

Symbol	Definition
MVR	Mean-to-variance ratio
M_i	Optimization metric M at the i_{th} iteration
F	Foreground/cell region
B	Background/substrate
σ_f^2	Foreground intensity variance
σ_b^2	Background intensity variance
μ_f	Foreground mean intensity value
μ_b	Background mean intensity value
G	Squared gradient magnitude of image
I_G	Spatial information/high intensity variation due to organelles in the cell
H	Normalized low pass Gaussian mask
I_F	Filtered Image
β	Erosion parameter

3.2 Convergence of the Metric

The convergence of metric M can be proven from experiments. Fig. 4 shows the metric M at each iteration for all objectives with/without filtering.

3.3 Spatial Information and Intensity Distribution

The hESC region, F, is a high intensity variation region while the substrate region, B, is a low intensity variation region. As a result, we are able to exploit the gradients of the image to segment out the cell region from the substrate region. The following equations show how we exploit the gradients of the image:

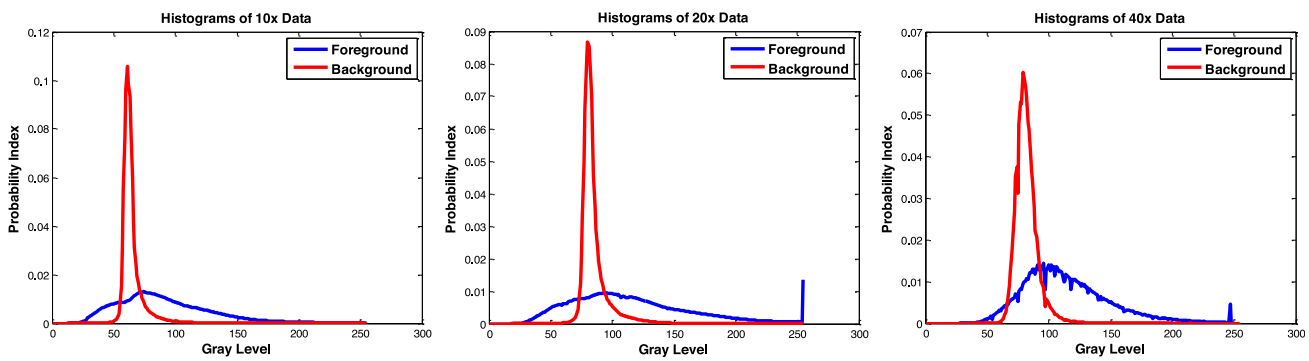

Fig. 2. Foreground and background intensity distributions for each data set.

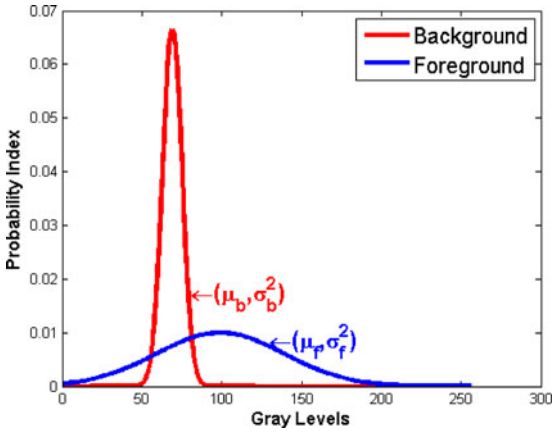

Fig. 3. Intensity distribution model of foreground and background.

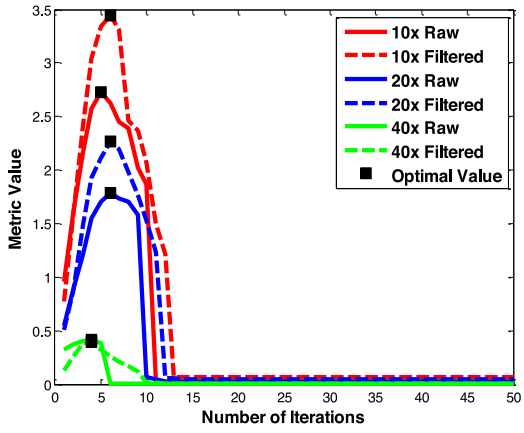

Fig. 4. Metric values at each iteration for images under different objectives.

$$I = F \cup B, \tag{6}$$

$$G = \left(\frac{dI}{dx}\right)^2 + \left(\frac{dI}{dy}\right)^2, \tag{7}$$

$$I_G = \log_e\left(\frac{(-1+e)\times G}{\max(G)} + 1\right) \times 255, \tag{8}$$

where G is the squared gradient magnitude of image, I. $\frac{dI}{dx}$ and $\frac{dI}{dy}$ are gradients of image, I, in the x and y directions, respectively. I_G is the spatial information produced by (8), which further emphasizes the difference between cell and substrate regions. Equation (8) normalizes G. The inner component of natural log transformation, $((-1+e)\times G/\max(G))+1$, ensures that the transformation result will be within the range from 0 to 1. When G is 0, then $\log_e(1)$ is equal to 0. When G is equal to the max of G, then $\log_e(e)$ is equal to 1 and I_G is equal to 255. The natural log function transforms a narrow range of small input values into a wider range of output values. Equation (8) is essentially a gamma correction technique [17]. It creates a large intensity separation between the foreground and background. Therefore, the natural log transformation enhances the image's intensity distribution to become a more visible bimodal distribution.

The proposed algorithm also uses a mean filter on I_G at each iteration to evolve the cell regions. It is able to group the cell region pixels together based on local information; the size of the mean filter dictates how fast the cell region is evolved. The method updates I_G and evolves the cell region until M is maximized.

Equation (4) is calculated based on the mean and variance of the intensity distributions of the cell and substrate data. The cell region, F, and substrate region, B, are updated by thresholding I_G with OTSU's method at each iteration [17]. The intensity distribution's mean and variance of the cell region and substrate region data are also updated at each iteration by the following equations:

$$\mu_f = \frac{\sum_{f\in F} f}{N_f}, \tag{9}$$

$$\mu_b = \frac{\sum_{b\in B} b}{N_b}, \tag{10}$$

$$\sigma_f^2 = \frac{\sum_{f\in F}(f-\mu_f)^2}{N_f}, \tag{11}$$

$$\sigma_b^2 = \frac{\sum_{b\in B}(b-\mu_b)^2}{N_b}, \tag{12}$$

where N_f and N_b are the total numbers of foreground and background pixels in the image, f and b are the intensity values in the corresponding foreground and background. Fig. 5 shows the intermediate and final results of the proposed method on various images. Figs. 5b, 5e, 5h and 5k show the spatial information when M_{opt} is reached for their respective data.

Input:
I: hESC phase contrast image.
β: erosion parameter.
Output:
F: the hESC region (foreground).
B: the substrate region (background).
Procedure Cell_Region_Detection(I,e);
{
1. Set $M_0 = 0$ & iteration $i \leftarrow 1$.
2. Calculate G and I_G with equations (7) and (8).
3. Update I_G by applying a mean filter to I_G from step 3 (spatial grouping).
4. Determine foreground and background regions F_1 and B_1 respectively by applying Otsu's method to I_G.
5. Calculate μ_f, μ_b, σ_f^2 and σ_b^2 using equations (9)-(12).
6. Calculate M_1 with equation (4).
7. While($M_i > M_{i-1}$){
   a) Iteration $i \leftarrow i+1$.
   b) Update I_G by applying a mean filter to I_G from the last iteration.
   c) Determine F_i and B_i regions by applying Otsu's method to I_G.
   d) Update μ_f, μ_b, σ_f^2 and σ_b^2 with equations (9)-(12).
   e) Update M_i with equation (4).
   }
8. F ← F_i .
9. B ← B_i.
10. Update F & B after morphological operation with ersion parameter β [17].
};

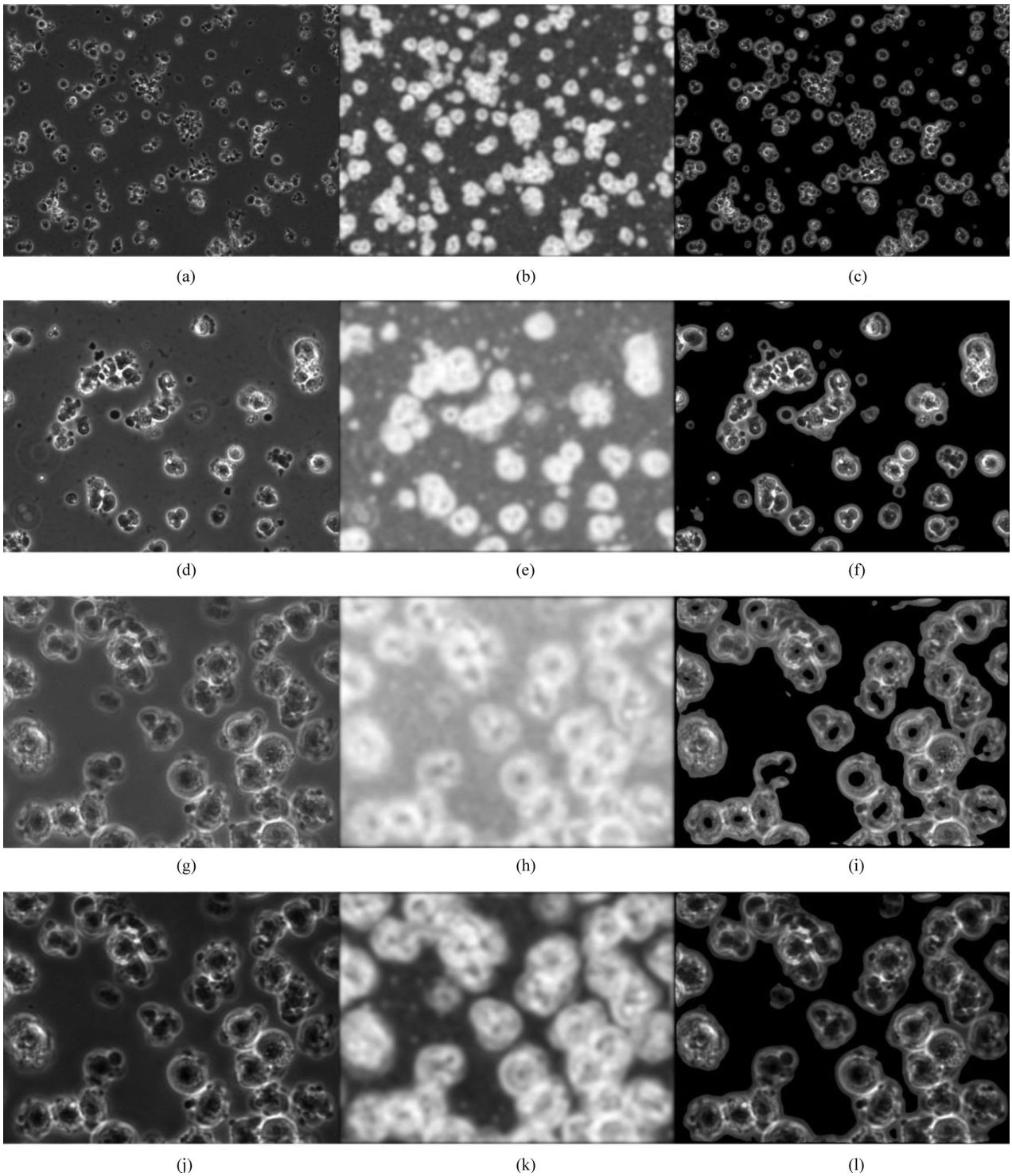

Fig. 5. (a) The original 10× image; (b) 10× image's spatial information at M_{opt}; (c) detected cell regions in 10× image; (d) The original 20× image; (e) 20× image's spatial information at M_{opt}; (f) detected cell regions in 20× image. (g) The original 40× image; (h) 40× image's spatial information at M_{opt}; (i) detected cell regions in 40× image. (j) The 40× image after the low pass Gaussian filter; (k) The filtered 40× image's spatial information at M_{opt}; (l) detected cell regions in the filtered 40× image.

3.4 Algorithm for Cell Region Detection

The algorithm for automated cell detection is given in the above. Note that I_G is updated in step 7.b) of the algorithm. We also use the same equations (9)-(12) to update μ_f, μ_b, σ_f^2 and σ_b^2 after the maximum M value. Our algorithm stops after the maximum is found. Fig. 4 shows what happens to the M value if the algorithm did not stop after the maximum M value is reached. It serves as an explanation why we can stop the algorithm when maximum M value is found. As shown in Fig. 4, M converges to zero after the maximum M value.

3.5 Noise Reduction

In some cases, the effect of system noise from the microscope is inevitably visible. One way to reduce the effect of noise in an image is to use a conventional filtering technique in the frequency or spatial domain. We use the low pass Gaussian mask to attenuate the noise in hESC images. This allows the improvement of detection accuracy. Fig. 6 shows the process and results of the filtering with a low pass Gaussian mask, H, and the equations for noise reduction technique are given below [17].

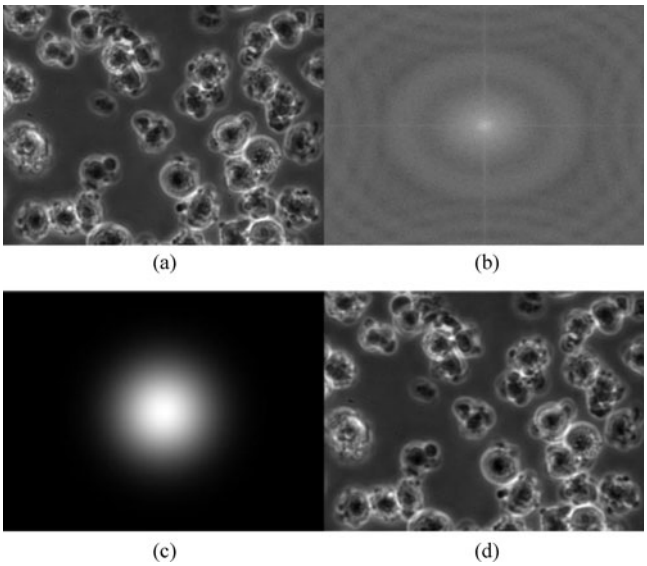

Fig. 6. (a) The original noisy 40× image; (b) noisy 40× image after 2D Fourier transformation; (c) low pass Gaussian mask with standard deviation equal to 80; (d) resulting image after noise filtering.

$$h_{gaus}(r,c) = e^{-\frac{(r-r_c)^2+(c-c_c)^2}{2\sigma^2_{gaus}}}, \tag{13}$$

$$H(r,c) = \frac{h_{gaus}(r,c)}{\sum_r \sum_c h_{gaus}(r,c)}, \tag{14}$$

$$I_F = \mathcal{F}^{-1}\{\mathcal{F}\{I\} \cdot \mathcal{F}\{H\}\}. \tag{15}$$

I_F and H have the same dimensionality as image, I, where it has R rows and C columns. $r \in \{1,..,R\}$ and $c \in \{1,..,C\}$. $h_{gaus}(r,c)$ is a low pass Gaussian mask value at location (r,c) and σ_{gaus} is the standard deviation of the Gaussian mask. (r_c, c_c) has the value $(R/2, C/2)$ which is the center location of the mask. $\mathcal{F}\{*\}$ is a 2D Fourier transform operation, and $\mathcal{F}^{-1}\{*\}$ is the inverse 2D Fourier transform operation.

3.6 Over-Segmentation Reduction

Since the mean filter is used to evolve the foreground region, over-segmentation is inevitable. Therefore, we use a morphological erosion technique to reduce the error caused by over-segmentation after the foreground and background regions have been detected [17]. In this paper, we use a common disk structuring element for the morphological erosion technique, and the erosion parameter is its radius. The erosion parameter is identified from a receiver operating characteristic (ROC) curve where a minimum of 90 percent true positive rate and a false positive rate (FPR) lower than 10 percent are achieved for each data set with/without filtering [18]. The first image of each data set is used to determine the erosion parameter and it is used for all the remaining images in a data set. The higher value of erosion parameter can lead to under-segmentation. However, if the erosion parameter is close to zero, over-segmentation can still exist. Since 40× image does not meet the above criteria, no erosion parameter is selected for it. Fig. 7 shows the ROC and the optimal points where the erosion parameters are picked.

The detected foreground and background regions have associated masks (binary images). The morphological erosion operation is applied to the foreground region with the erosion parameter found from Fig. 7. Since the foreground and background regions are complement of each other, the updated background region can be derived directly from the updated foreground region.

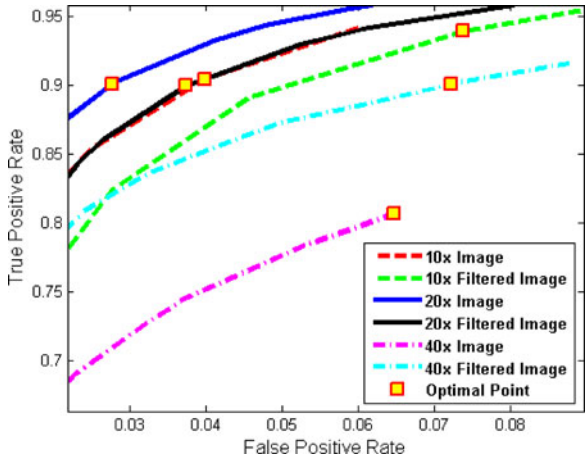

Fig. 7. ROC plots for images under different objectives with varying erosion parameter.

4 Experimental Results

4.1 Data

All time lapse videos were obtained with a BioStation IM [19]. The frames in the video are phase contrast images with 600 × 800 resolution. The videos were acquired using three different objectives: 10×, 20× and 40× and each objective has a set of 40 images, with a total of 120 images. Each video frame is taken roughly 2 minutes apart for the purpose of data variation from frame to frame. The ground-truth is generated manually by the expert biologists.

Note that for all the video data used in this paper, the hESC culture conditions are considered to be excellent. All videos used are of small colonies or single hESC, and the cells look excellent for unattached hESCs and colonies. Most hESC culture today is not done on mouse embryonic fibroblasts (MEFs). We have not cultured hESC on feeders since 2008. We use mTeSR medium [20]. This modern culture media does not require the use of MEFs, so they are seldom used. With an exception for maintenance, MEFs are not used in experiments. Since it is highly unlikely that we will analyze hESC cultured on MEFs, we have not tested our algorithms on data sets with hESC cultured on MEFs. Moreover, the images in this manuscript have very few dead cells and debris. In fact, they are remarkably clean considering the cells have been stripped and replated.

4.2 Parameters

Each video collected with different objectives has a different default size of neighborhood for spatial grouping. The default sizes are determined by observing the ROC plots with various window sizes for each objective. Based on the experimental analysis in [13], we concluded that the optimal neighborhood sizes for 10×, 20× and 40× are 5 × 5, 7 × 7 and 11 × 11, respectively. The selection criteria for the neighborhood sizes are based on finding a window for which its ROC plot yields a high true positive rate while keeping the low false positive rate. A low pass Gaussian mask with a standard deviation equal to 80 pixels is used to get rid of the noise that occurs during the video acquisition process. For the erosion parameter which is discussed in Section 3.6, we use a disk with radius 2, 5, 4, 8, 0, and 1 for 10×, filtered 10, 20, filtered 20×, 40× and filtered 40× data sets, respectively.

4.3 Performance Measures

The true positive, TP, is the overlapped region between the detected cell region and the cell region ground-truth. True negative, TN, is the overlapped region between the detected

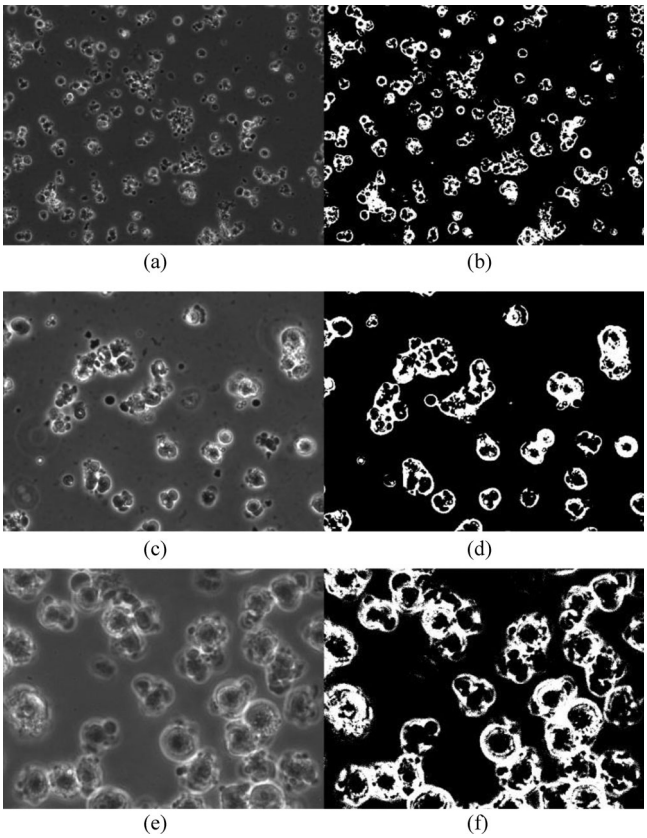

Fig. 8. (a) The original 10× image; (b) binary result of (a) with Otsu's; (c) the original 20× image; (d) binary result of (c) with Otsu's; (e) the original 40× image; (f) binary result of (e) with Otsu's.

background region and the background ground-truth. The false positive, FP, is the detected background that is falsely identified as part of the cell region. The false negative, FN, is the detected cell region that is falsely identified as part of the background.

The true positive rate or sensitivity, TPR or SEN, measures the proportion of actual positives which are correctly identified:

$$TPR = \frac{TP}{(TP + FN)}. \tag{16}$$

The false positive rate, measures the proportion of false positives which are incorrectly identified:

$$FPR = \frac{FP}{(FP + TN)}. \tag{17}$$

The specificity, SPC, is the true negative rate which is a complement of false positive rate:

$$SPC = \frac{TN}{(FP + TN)}. \tag{18}$$

The Jaccard similarity, JAC, is a measure of similarity between experimental results and the ground-truth:

$$JAC = \frac{TP}{(TP + FP + FN)}. \tag{19}$$

The Dice coefficient, DIC, measures the agreement between experimental results and ground-truth:

$$DIC = \frac{2TP}{(2TP + FP + FN)}. \tag{20}$$

TABLE 2
Comparisons of 10× Data Set (* Denotes Filtered Data)

Method	Jaccard	Dice	SEN	SPC
Proposed	**0.737**	**0.848**	**0.907**	**0.911**
Proposed*	**0.728**	**0.843**	**0.905**	**0.907**
KM	0.465	0.635	0.519	0.956
KM*	0.403	0.574	0.428	0.977
MGEM	0.608	0.756	0.793	0.884
MGEM*	0.591	0.743	0.852	0.831
CLQuant with 10x recipe	0.674	0.806	0.722	0.973
CLQuant* with 10x recipe	0.579	0.734	0.610	0.980
CLQuant with 20x recipe	0.622	0.767	0.978	0.781
CLQuant* with 20x recipe	0.538	0.700	0.988	0.680
CLQuant with 40x recipe	0.558	0.716	0.918	0.753
CLQuant* with 40x recipe	0.477	0.646	0.916	0.648

The average detection error is an average of type I (1-SPC) and type II (1-SEN). ANOVA test [21] is also used for comparison of detected foreground and background intensity distributions with the corresponding ground-truth intensity distributions.

4.4 Methods Compared

We compared the proposed method with k-means, Mixture of Gaussians, and CL-Quant software with various recipes [7], [10], [14]. In addition, we evaluated the data sets with Otsu's algorithm [17]. However, it was not able to detect the entire cell region due to fact that the intensity values of the cell body are similar to the substrate intensity values. As shown in Fig. 8, the result was not useful. Therefore, Otsu's algorithm is not compared in this paper.

Note that we do not compare this work with our work in reference [5] which is concerned with the growth of attached hESCs. This is quite different from the current study. In this study, the images are comprised of single cells and small colonies. The small colonies are cell colonies that contain more than two cells. From image processing point of view, the detection of large cell colonies is much easier than detection of all individual cell regions in the low cell confluence images. We are not focused with the detection of large cell colonies in this paper. Here we are concerned with using basic image properties of hESCs to extract individual cell regions. The detection algorithm exploits the *high* intensity variation within the cell body due to the presence of organelles. Most importantly, CLQuant is able to detect the large cell colonies after training as discussed [5]. However, the data sets used in this paper are much more challenging to CLQuant even after *extensive* training.

TABLE 3
Comparisions of 20× Data Set (* Denotes Filtered Data)

Method	Jaccard	Dice	SEN	SPC
Proposed	**0.754**	**0.860**	**0.906**	**0.924**
Proposed*	**0.739**	**0.850**	**0.908**	**0.914**
KM	0.446	0.617	0.516	0.941
KM*	0.358	0.527	0.378	0.978
MGEM	0.585	0.738	0.804	0.859
MGEM*	0.581	0.735	0.827	0.840
CLQuant with 10x recipe	0.689	0.816	0.767	0.958
CLQuant* with 10x recipe	0.652	0.789	0.709	0.967
CLQuant with 20x recipe	0.663	0.797	0.797	0.924
CLQuant* with 20x recipe	0.600	0.750	0.860	0.837
CLQuant with 40x recipe	0.596	0.747	0.915	0.799
CLQuant* with 40x recipe	0.547	0.707	0.932	0.735

TABLE 4
Comparisons of 40× Data Set (* Denotes Filtered Data)

Method	Jaccard	Dice	SEN	SPC
Proposed	**0.735**	**0.847**	**0.749**	**0.968**
Proposed*	**0.866**	**0.928**	**0.902**	**0.931**
KM	0.674	0.805	0.797	0.697
KM*	0.411	0.583	0.412	0.995
MGEM	0.621	0.766	0.634	0.963
MGEM*	0.775	0.874	0.827	0.890
CLQuant with 10x recipe	0.724	0.840	0.734	0.976
CLQuant* with 10x recipe	0.567	0.724	0.569	0.994
CLQuant with 20x recipe	0.792	0.884	0.885	0.803
CLQuant* with 20x recipe	0.737	0.849	0.801	0.855
CLQuant with 40x recipe	0.831	0.908	0.952	0.758
CLQuant* with 40x recipe	0.805	0.892	0.930	0.741

TABLE 5
Average Detection Errors of Foreground and Background

Data	K-means	MGEM	CL Quant with 10x Recipe	CL Quant with 20x Recipe	CL Quant with 40x Recipe	Proposed
10x Data	26.28%	16.18%	15.26%	12.05%	16.46%	**9.07%**
10x Data (Filtered)	29.79%	15.84%	20.51%	16.61%	21.80%	**9.41%**
20x Data	27.15%	16.83%	13.77%	13.96%	14.34%	**8.47%**
20x Data (Filtered)	32.16%	16.62%	16.20%	15.16%	16.62%	**8.90%**
40x Data	25.33%	20.14%	14.46%	15.60%	14.50%	**14.17%**
40x Data (Filtered)	29.64%	14.17%	21.84%	17.20%	16.46%	**8.36%**

4.5 Results and Discussion

The proposed method was tested with three videos (each with 40 frames) that were acquired with 10×, 20× and 40× objectives. The proposed method achieved above 90 percent in sensitivity and specificity on 10× with/without filtering, 20× with/without filtering and 40× with filtering data sets. Since pre-filtering gets rid of high frequency noise, it improves the performance of the proposed algorithm on noisy data. The 10 and 20× data sets are not corrupted with high frequency noise. Therefore, pre-filtering on those data sets would not affect the algorithm's performance on JAC, DIC, SEN and SPC measures as shown in Tables 2 and 3. However, the 40× data set is corrupted with high frequency noise. The pre-filtering improves the yield on its SEN measure significantly as shown in Table 4.

In this paper, we compared the proposed method with K-means, mixture of Gaussians segmentation method and CL-Quant software under different recipes. Tables 2, 3, and 4 show the results of the K-means, MGEM segmentation, CL-Quant software, and the proposed method on all experimental data. The proposed method outperforms the other methods in JAC and DIC measures. Moreover, the proposed method yields above

Anova Test on 10X's Data Results by the Proposed Method without Filtering

Foreground Distribution

'Source'	'SS'	'df'	'MS'	'F'	'Prob>F'
'Columns'	3.02E+11	255	1.19E+09	37.25	0
'Error'	8.15E+09	256	3.18E+07	[]	[]
'Total'	3.10E+11	511	[]	[]	[]

Background Distribution

'Source'	'SS'	'df'	'MS'	'F'	'Prob>F'
'Columns'	2.30E+13	255	9.01E+10	2831.21	0
'Error'	8.15E+09	256	3.18E+07	[]	[]
'Total'	2.30E+13	511	[]	[]	[]

Anova Test on 10X's Data Results by the Proposed Method with Filtering

Foreground Distribution

'Source'	'SS'	'df'	'MS'	'F'	'Prob>F'
'Columns'	3.11E+11	255	1.22E+09	32.07	0
'Error'	9.73E+09	256	3.80E+07	[]	[]
'Total'	3.21E+11	511	[]	[]	[]

Background Distribution

'Source'	'SS'	'df'	'MS'	'F'	'Prob>F'
'Columns'	2.30E+13	255	9.00E+10	2368.96	0
'Error'	9.73E+09	256	3.80E+07	[]	[]
'Total'	2.30E+13	511	[]	[]	[]

Anova Test on 20X's Data Results by the Proposed Method without Filtering

Foreground Distribution

'Source'	'SS'	'df'	'MS'	'F'	'Prob>F'
'Columns'	1.84E+11	255	7.20E+08	32.75	0
'Error'	5.63E+09	256	2.20E+07	[]	[]
'Total'	1.89E+11	511	[]	[]	[]

Background Distribution

'Source'	'SS'	'df'	'MS'	'F'	'Prob>F'
'Columns'	1.83E+13	255	7.16E+10	3255.54	0
'Error'	5.63E+09	256	2.20E+07	[]	[]
'Total'	1.83E+13	511	[]	[]	[]

Anova Test on 20X's Data Results by the Proposed Method with Filtering

Foreground Distribution

'Source'	'SS'	'df'	'MS'	'F'	'Prob>F'
'Columns'	1.93E+11	255	7.56E+08	27.16	0
'Error'	7.13E+09	256	2.78E+07	[]	[]
'Total'	2.00E+11	511	[]	[]	[]

Background Distribution

'Source'	'SS'	'df'	'MS'	'F'	'Prob>F'
'Columns'	1.82E+13	255	7.13E+10	2562.46	0
'Error'	7.13E+09	256	2.78E+07	[]	[]
'Total'	1.82E+13	511	[]	[]	[]

Anova Test on 40X's Data Results by the Proposed Method without Filtering

Foreground Distribution

'Source'	'SS'	'df'	'MS'	'F'	'Prob>F'
'Columns'	1.10E+12	255	4.30E+09	18.21	0
'Error'	6.04E+10	256	2.36E+08	[]	[]
'Total'	1.16E+12	511	[]	[]	[]

Background Distribution

'Source'	'SS'	'df'	'MS'	'F'	'Prob>F'
'Columns'	4.22E+12	255	1.65E+10	70.10	0
'Error'	6.04E+10	256	2.36E+08	[]	[]
'Total'	4.28E+12	511	[]	[]	[]

Anova Test on 40X's Data Results by the Proposed Method with Filtering

Foreground Distribution

'Source'	'SS'	'df'	'MS'	'F'	'Prob>F'
'Columns'	1.33E+12	255	5.23E+09	253.49	0
'Error'	5.28E+09	256	2.06E+07	[]	[]
'Total'	1.34E+12	511	[]	[]	[]

Background Distribution

'Source'	'SS'	'df'	'MS'	'F'	'Prob>F'
'Columns'	3.77E+12	255	1.48E+10	716.63	0
'Error'	5.28E+09	256	2.06E+07	[]	[]
'Total'	3.78E+12	511	[]	[]	[]

Fig. 9. ANOVA test of foreground and background distributions for all data sets. SS = sum of squares, df = degree of freedom, MS = mean square, F = F-statistic, [] = not applicable.

90 percent in both SEN and SPC measures. K-means clusters the image data based only on the nearest mean while the MGEM method groups the data solely on the modeled intensity distribution. Consequently, neither method was able to detect the entire cell regions. Instead, they have detected fragments of the actual cell regions. Their performance is further degraded by the presence of noise. The CL-Quant software's performance depends heavily on the recipe maker. The recipes for the data sets used in this paper are created by a fourth year biology PhD student. More importantly, the proposed method's performance is good on the image data with or without filtering.

In terms of performance, the proposed method yields lower than 10 percent average detection error of foreground and background on 10 and 20× with/without filtering, and 40× with filtering data sets as shown in Table 5. MGEM has a minimum of 14.17 percent and a maximum of 20.14 percent average detection error [10]. K-means algorithm yields above 25 percent average detection error on all data sets [7]. CL-Quant gives a minimum of 12.05 percent and a maximum of 21.84 percent average detection error [14]. In terms of convergence, the proposed method converges in seven iterations on the average, and each iteration requires 0.17 second. It reaches the global optimum since the mean filter is used for grouping similar regions in the algorithm.

5 Conclusions

The proposed method incorporated the concept of local property of a hESC as well as cell and substrate intensity distributions for cell region detection in phase contrast images. It uses the spatial information to improve the connectivity of local pixels to their corresponding regions. More importantly, it enables fast convergence to the maximum absolute difference of foreground and background mean-to-variance ratios. The proposed method is able to split the image data into two Gaussian distributions; intensity distribution of the foreground and background data. Table 5 shows that the proposed method yields a lower average detection error than the K-means, MGEM and CL-Quant methods [7], [10], [14]. Fig. 9 shows an ANOVA test for all experimental data sets. It shows low error in comparison between the intensity distributions of the proposed method and the ground-truth intensity distributions. In the case of noisy images, the pre-filtering of the image data can greatly improve the performance of the algorithm. In term of speed, the proposed method converges in less than 1.2 seconds while K-means and MGEM take about 3.61 and 25.3 seconds respectively on a laptop with a Intel(R) Core 2 Duo CPU processor that run at 2.53 GHz. The CL-Quant software requires at least six minutes of user inputs from the expert biologist for each recipe. Application of this automated method to hESC will facilitate the analysis of their dynamic behaviors and benefit research in both regenerative and preventive medicine.

It is to be noted that the proposed method studies single cells and small colonies after plating before the cells are attached. Differentiation would not be a factor unless cells are first attached and then incubated for at least 24 hours in a medium that supports differentiation. Our method works on cells that have high intensity variation on their cell bodies. As long as this image property still holds for dead cells, differentiated and undifferentiated/pluripotent hESCs, we can detect them. The proposed cell region detection is a start for an automated cell region detection and cell classification. With the automated cell region detection, we can move forward our research for an automated classification system.

Acknowledgments

This research was supported by NSF-IGERT: Video Bioinformatics Grant DGE 0903667 and by Tobacco-Related Disease Research Program (TRDRP): Grant 20XT-0118 and by a TRDRP Postdoctoral Fellowship (20FT-0084). The authors would like to thank Jo-Hao Weng for making the CL-Quant software recipes.

References

[1] J.A. Thomson et al., "Embryonic Stem Cell Lines Drived from Human Blastocysts," *Science*, vol. 282, no. 5395, pp. 1145-1147, Nov. 1998.
[2] J. Nichols and A. Smith, "The Original and Identity of Embryonic Stem Cells," *Development*, vol. 138, pp. 3-8, Jan. 2011.
[3] M. Stojkovic, M. Lako, T. Strachan, and A. Murdoch, "Derivation, Growth and Applications of Human Embryonic Stem Cells," *Reproduction*, vol. 128, pp. 259-267, Sept. 2004.
[4] P. Talbot and S. Lin, "Mouse and Human Embryonic Stem Cells: Can They Improve Human Health by Preventing Disease?" *Current Topics in Medicinal Chemistry*, vol. 11, no. 13, pp. 1638-1652, 2011.
[5] S. Lin et al., "Comparison of the Toxicity of Smoke from Conventional and Harm Reduction Cigarettes Using Human Embryonic Stem Cells," *Toxicol Science*, vol. 118, pp. 202-212, Aug. 2010.
[6] S. Lin et al., "Video Bioinformatics Analysis of Human Embryonic Stem Cell Colony Growth," *J. Visualized Experiments*, vol. 39, pp. 1-5, May 2010.
[7] S. Tatiraju and A. Mehta, "Image Segmentation Using K-Means Clustering, EM and Normalized Cuts," pp. 1-7, http://www.ics.uci.edu/~dramanan/teaching/ics273a_winter08/projects/avim_report.pdf, UC Irvine, 2008.
[8] K. Alsabti, S. Ranka, and V. Singh, "A Efficient K-Means Clustering Algorithm," *Proc. First Workshop High Performance Data Mining*, 1998.
[9] T. Kanungo, D.M. Mount, N.S. Netanyahu, C.D. Piatko, R. Silverman, and A.Y. Wu, "An Efficient K-Means Clustering Algorithm: Analysis and Implementation," *IEEE Trans. Pattern Analysis and Machine Intelligence*, vol. 24, no. 7, pp. 881-892, July 2002.
[10] R. Farnoosh and B. Zarpak, "Image Segmentation Using Gaussian Mixture Model," *Int'l J. Eng. Science*, vol. 19, pp. 29-32, 2008.
[11] L. Xu and M.I. Jordan, "On Convergence Properties of the EM Algorithm for Gaussian Mixture," *Neural Computation*, vol. 8, pp. 129-151, 1996.
[12] S. Gopinath, Q. Wen, N. Thakoor, K. Luby-Phelps, and J.X. Gao, "A Statistical Approach for Intensity Loss Compensation of Confocal Microscopy Images," *J. Microscopy*, vol. 230, pp. 143-159, 2008.
[13] B.X. Guan, B. Bhanu, P. Talbot, and S. Lin, "Automated Human Embryonic Stem Cell Detection," *Proc. IEEE Second Int'l Conf. Healthcare Informatics, Imaging and Systems Biology*, pp. 75-82, Sept. 2012.
[14] Nikon. CL-Quant, http://www.nikoninstruments.com/News/US-News/Nikon-Instruments-Introduces-CL-Quant-Automated-Image-Analysis-Software, July 2013.
[15] S. Lin and P. Talbot, "Methods for Culturing Mouse and Human Embryonic Stem Cells," *Methods Molecular Biology*, vol. 690, pp. 31-56, 2011.
[16] J. Bushberg, J. Seibert, E. Leidholdt, and J. Boone, *The Essential Physics of Medical Imaging*. second ed., Lippincott William & Wilkins, 2002.
[17] R.C. Gonzalez and R.E. Woods, *Digital Image Processing*, third ed., pp. 627-794. Pearson Education Inc, 2008.
[18] M. Pepe, G.M. Longton, and H. Janes, "Comparison of Receiver Operating Characteristics Curves," *UW Biostatistics Working Paper Series-Working Paper 323 eLetter*, http://biostats.bepress.com/uwbiostat/paper323, Jan. 2008.
[19] Nikon, Biostation-IM, http://www.nikoninstruments.com/Vyrobky/Cell-Incubator- Observation/BioStation-IM, Nov. 2012.
[20] StemCell Technologies, mTeSR Medium, http://www.stemcell.com/en/Products/Popular-Product-Lines/mTeSR-TeSR2.aspx, Jan. 2014.
[21] R.V. Hogg and J. Ledolter, *Engineering Statistics*. MacMillan, 1987.